Geophysical Research Letters

RESEARCH LETTER
10.1029/2020GL089035

Special Section:
The COVID-19 Pandemic: Linking Health, Society and Environment

COVID-19 Impact on the Concentration and Composition of Submicron Particulate Matter in a Typical City of Northwest China

Jianzhong Xu[1], Xinlei Ge[2], Xinghua Zhang[1], Wenhui Zhao[1], Ruixiong Zhang[3], and Yuzhong Zhang[4]

[1]State Key Laboratory of Cryospheric Science, Northwest Institute of Eco-Environment and Resources, Chinese Academy of Sciences, Lanzhou, China, [2]Jiangsu Key Laboratory of Atmospheric Environment Monitoring and Pollution Control, Collaborative Innovation Center of Atmospheric Environment and Equipment Technology, School of Environmental Science and Engineering, Nanjing University of Information Science and Technology, Nanjing, China, [3]School of Earth and Atmospheric Sciences, Georgia Institute of Technology, Atlanta, GA, USA, [4]School of Engineering, Westlake University, Hangzhou, China

Abstract In this study, we evaluated the variations of air quality in Lanzhou, a typical city in Northwestern China impacted by the COVID-19 lockdown. The mass concentration and chemical composition of non-refractory submicron particulate matter (NR-PM_1) were determined by a high-resolution aerosol mass spectrometer during January-March 2020. The concentration of NR-PM_1 dropped by 50% from before to during control period. The five aerosol components (sulfate, nitrate, ammonium, chloride, and organic aerosol [OA]) all decreased during the control period with the biggest decrease observed for secondary inorganic species (70% of the total reduction). Though the mass concentration of OA decreased during the control period, its source emissions varied differently. OA from coal and biomass burning remained stable from before to during control period, while traffic and cooking related emissions were reduced by 25% and 50%, respectively. The low concentration during the control period was attributed to the lower production rate for secondary aerosols.

Plain Language Summary At the beginning of 2020, a novel coronavirus disease (COVID-19) was spreading in China and lasting through the following months. People's outdoor activities due to the coupling effect of this epidemic and the Chinese New Year holiday were greatly reduced and pollutant emissions related with these activities were also reduced during this period. This situation provides us a unique chance to look into the air quality and evaluate the corresponding mitigation measures in the city. We observed a significant drop of the mass concentration of NR-PM_1 by 50% in Lanzhou. The reduction of NR-PM_1 was mainly from secondary inorganic species accounting for 70% of reduced NR-PM_1. This finding is significantly different from that observed in Eastern China where the mass concentration of fine particulate matter was not reduced significantly with the reduction of primary emissions due to enhanced secondary production. In contrast, the production rates for secondary inorganic and organic aerosols showed a decreasing trend from before to during control period. These results revealed the large difference in air pollution chemistry between East and West China.

Key Points:
- The submicron aerosol mass concentration was reduced by 50% during COVID-19 lockdown in Lanzhou
- The reduction of aerosol was mainly due to a decline in secondary species; we identify an overall low production rate as the main driver
- The result is contrast to those reported recently in East China where the reductions were offset by an increase in secondary species production

Supporting Information:
- Supporting Information S1

Correspondence to:
J. Xu and X. Ge,
jzxu@lzb.ac.cn;
caxinra@163.com

Citation:
Xu, J., Ge, X., Zhang, X., Zhao, W., Zhang, R., & Zhang, Y. (2020). COVID-19 impact on the concentration and composition of submicron particulate matter in a typical city of Northwest China. *Geophysical Research Letters*, *47*, e2020GL089035. https://doi.org/10.1029/2020GL089035

Received 27 MAY 2020
Accepted 8 SEP 2020
Accepted article online 25 SEP 2020

1. Introduction

Lanzhou, locating in the northwest part of China, is the capital of Gansu province and a typical city of northwestern China with coal combustion as the major fuel for residential heating during winter. Increased energy consumption and fast urbanization in past decades have aggravated its air pollution. In recent 10 years, many great efforts have been conducted by the local government to improve the air quality, and great achievement was reached (http://www.gov.cn/zwgk/2013-09/12/content_2486773.htm). Xu et al. (2016) presented an intensive study during wintertime in Lanzhou and demonstrated the improvement of air quality in this city comparing with its past. For Lanzhou, the chemical composition of nonrefractory submicron particulate matter (NR-PM_1) was mainly dominated by organic aerosol (OA, 51%), nitrate (17%), and sulfate (13%); the primary sources of OA included traffic, coal and biomass combustion, and cooking emissions, while the secondary species were dominated by photochemical production.

During the winter of 2019, the same group conducted a study to monitor the spatial distribution of air pollutants of this city via the mobile measurement by using a suite of online instruments. Ten days before the Chinese New Year (CNY, 25 January 2020), the vehicle was stopped at the Yard of Northwest Institute of Eco-Environment and Resources, and to stationarily monitor the air pollutants (Figure S1 in the supporting information). The measurement lasted from 14 January to 4 March 2020, which cover the periods of before and during the lockdown due to Coronavirus Disease 2019 (COVID-19) pandemic (Tian et al., 2020). The life pattern of residents in this city and the primary emissions of air pollutants during COVID-19 lockdown were greatly different from their normal states. This work provides a unique and timely investigation of the NR-PM_1 concentration and furthermore chemical composition, source contributions under different scenarios owing to the COVID-19 lockdown.

2. Materials and Methods

The instruments placed inside the mobile truck included an Aerodyne high-resolution time-of-flight mass spectrometer (HR-ToF-AMS, Aerodyne, Inc., Billerica, MA, USA) (Canagaratna et al., 2007; DeCarlo et al., 2006), a scanning mobility particle sizer (SMPS, Model 3936, TSI Inc., Shoreview, MN, USA), and a carbon dioxide (CO_2) sensor (Model 840A, LICOR, USA). The inlet used a $PM_{2.5}$ cyclone to cut off the coarse PM. Before sampling by each instrument, the air flow was dried by a Nafion dyer; therefore, the relative humidity was kept below 15% during the study. The HR-ToF-AMS was operated under only V-mode with 5 min resolution. The CO_2 recorded data at 1 s resolution, which were converted to 5 min resolution later for consistency.

All instruments were calibrated before sampling following standard methods. For example, the HR-ToF-AMS was calibrated for its flow rate, size, and ionization efficiency (IE) following the procedures described in Jayne et al. (2000); The IE calibration was conducted using NH_4NO_3 and $(NH_4)_2SO_4$ for ammonium and sulfate, respectively. The CO_2 monitor was calibrated using the high-precision and high-accuracy CO_2 standard gas.

Data preprocessing was mainly conducted on HR-ToF-AMS data using the standard software, that is, SQUIRREL (V1.63) and PIKA (V1.23) written in IGOR Pro (Wavemetrics Inc., OR, USA; http://cires.colorado.edu/jimenez-group/ToFAMSResources/ToFSoftware/index.html). An empirical particle collection efficiency (CE) of 0.5 was used, which was validated using composition-dependent CE included in software. These two CE results were highly consistent. The CE was also verified by the intercomparison between SMPS and HR-ToF-AMS volume data which showed a tight correlation and a slope within instrumental uncertainties, especially considering the different size ranges sampled by each instrument (Figure S2). The density for each NR-PM_1 inorganic component in calculating its volume was adopt from Zhang et al. (2005) and organics from elemental ratio method (Canagaratna et al., 2015; Kuwata et al., 2011). Default relative ionization efficiency (RIE) values were used for organics (1.4), nitrate (1.1), and chloride (1.3), while an RIE value of 4.1 was determined for ammonium and 1.38 for sulfate based on the calibrations of pure NH_4NO_3 and $(NH_4)_2SO_4$, respectively. The source apportionment of OA was first conducted by positive matrix factorization (PMF) with the robust engine (Paatero and Tapper, 1994) and explored using the PMF Evaluation Tool (Ulbrich et al., 2009); however, some factors were not properly resolved. The five-factor to seven-factor solutions are shown in the supporting information (Figures S3–S5). A SoFi (solution finder) toolkit using ME2 engine was then used to further explore the PMF solutions by using *a*-value approaching (Canonaco et al., 2013). Six factors were finally identified including traffic emitted OA (HOA), biomass burning emitted OA (BBOA), coal combustion OA (CCOA), cooking-related OA (COA), low-oxidized oxygenated OA (LO-OOA), and more-oxidized oxygenated OA (MO-OOA) (Figure S6). Technical details can be found in our previous publications (Xu et al., 2014, 2016).

3. Results and Discussion

3.1. Variations of PM Mass Concentration Before and During the COVID-19 Lockdown

Considering the different life patterns during the study, the sampling period was divided into four periods, that is, normal period (P1, 14–17 January 2020), the CNY holiday period (P2, 18 January to 4 February 2020), strict control period (P3, 5–16 February 2020), and recovery period (P4, 17 February to 4 March 2020). The life pattern during P1 in the city that was 1 week before CNY was normal with high anthropogenic activities

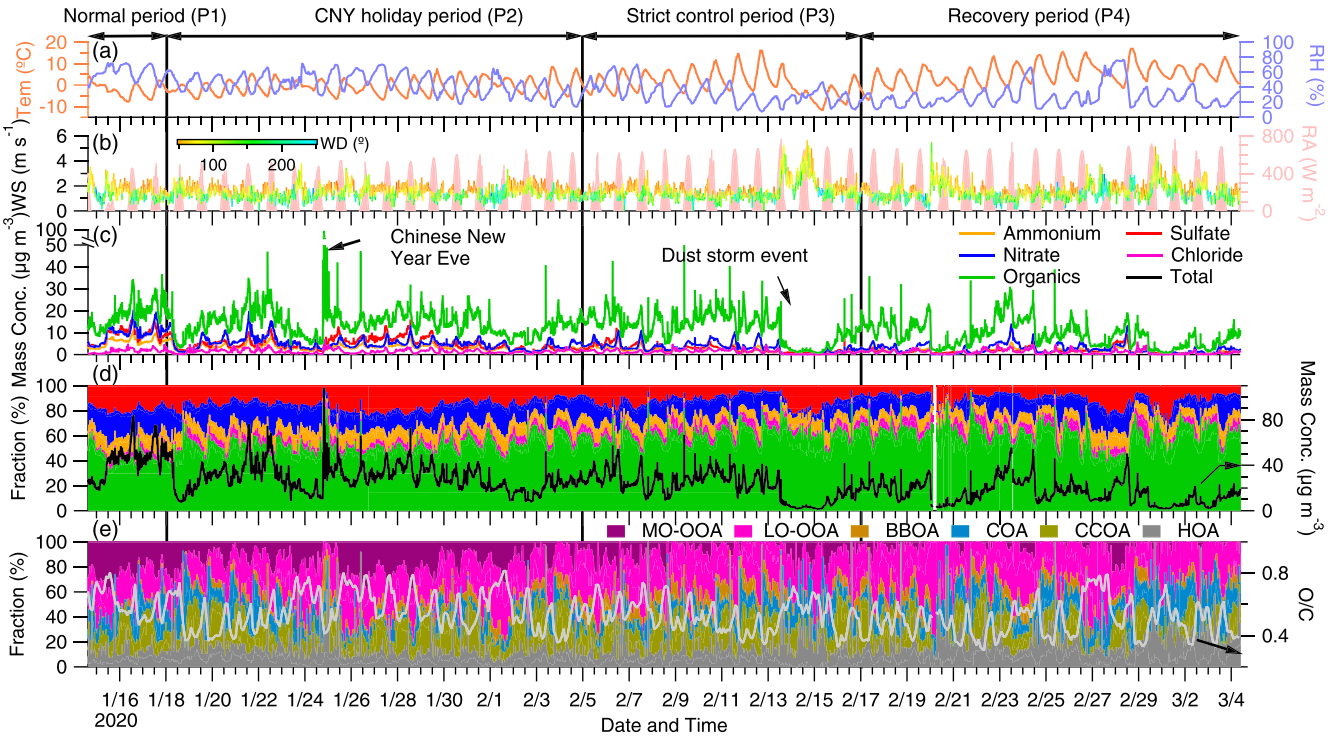

Figure 1. Overview plot of meteorological data and HR-ToF-AMS data. Time series of (a) air temperature (Tem) and relative humidity (RH), (b) wind speed (WS) colored by wind direction (WD) and solar radiation (RA), (c) AMS components and total NR-PM_1, (d) the contribution of each AMS components, and (e) the contribution of organic aerosol components and oxygen-to-carbon (O/C) ratio of OA at 1 hr resolution. The vertical solid lines divide the sampling period into four periods.

and PM mass concentration (Figure 1). During P2, many people left for the CNY for a 3 week-long holiday. The concentration of air pollutants was distinctly reduced at the beginning of P2 (Figure 1). The COVID-19 lockdown was first imposed in 23 January in Wuhan city (the epicenter of COVID-19 outbreak in China), and the local government of Lanzhou also issued measures to constrain the spread of the pandemic. People inside the city therefore reduced their outdoor activities, and a portion of commercial stores were also closed. During P3, with the increase of confirmed COVID-19 cases in China and Lanzhou, people were restricted to stay at home; therefore outdoor activities almost vanished, but instead, household activities were likely enhanced during this period. For example, in order to maintain warm conditions in home, the usage of coal from communities and central heating plants likely increase. During P4, with the decreased cases of COVID-19, the government encouraged people to gradually return to work; thus, the traffic and other anthropogenic activities gradually resumed. Overall, the P1 could be treated as a reference period with intense primary emissions, while these emissions during P2, P3, and P4 were all reduced but to different extents.

The meteorological data, chemical composition, and mass concentration of NR-PM_1 observed in this study were all shown in Figure 1. Note the data below are the arithmetic mean of each period. From P1 to P4, the wind conditions are quite stable with low wind speed (mean values: ~1.5 m s^{-1}; Table 1) and dominating wind directions from eastern to northeastern (Figure S7). Air trajectory analysis also showed similar westerly dominated air masses throughout the sampling period (Figure S8). The average air temperature increased step by step from −2.26°C (P1) to 5.15°C (P4) as well as solar radiation (Figure 1a), while the relative humidity continuously decreased from ~60% (P1) to 28% (P4). Overall, these results indicated a warmer and dryer weather conditions transited from P1 to P4 yet calm and similar wind conditions. The mass concentration of NR-PM_1 showed an evidently decreasing trend from P1 (46.5 μg m^{-3}) to P4 (15.8 μg m^{-3}) with a reduction rate of 52.3% from before (P1) to during pandemic (P2–P4) (Figure 2a). The mass concentration of NR-PM_1 during recovery period (P4) in Lanzhou did not increase, probably owing to the overall limited

Table 1
The Meteorological Conditions During Different Periods

	P1P1	**P2**P2	**P3**P3	**P4**P4
Wind speed (m s^{-1})	1.53 ± 0.57	1.50 ± 0.48	1.59 ± 0.78	1.57 ± 0.64
Air temperature (°C)	−2.26 ± 2.99	−0.68 ± 3.40	1.07 ± 5.44	5.15 ± 4.9
Relatively humidity (%)	59.95 ± 9.24	44.74 ± 13.58	3,099 ± 14.02	27.78 ± 14.7
Solar radiation (W m^{-2})	82.18 ± 145.67	118.79 ± 185.3	156.0 ± 230.3	162.4 ± 236.8
Sulfate	9.53 ± 2.94	4.86 ± 2.51	2.66 ± 1.89	1.66 ± 1.20
Nitrate	10.28 ± 3.37	5.06 ± 2.65	3.42 ± 2.34	2.49 ± 2.05
Chloride	1.78 ± 0.87	1.43 ± 0.84	1.29 ± 0.90	1.09 ± 0.95
Ammonium	6.16 ± 1.73	3.26 ± 1.37	2.12 ± 1.26	1.58 ± 1.03
HOA	1.60 ± 1.03	1.34 ± 2.01	1.18 ± 1.91	1.19 ± 1.60
COA	2.88 ± 3.23	1.56 ± 1.83	1.38 ± 1.33	1.35 ± 1.06
BBOA	0.35 ± 0.42	0.92 ± 1.78	1.29 ± 1.01	0.77 ± 0.78
CCOA	3.32 ± 1.98	2.85 ± 2.09	2.54 ± 2.19	1.69 ± 1.75
LO-OOA	4.07 ± 2.05	4.06 ± 1.89	4.10 ± 2.62	2.76 ± 2.20
MO-OOA	6.51 ± 2.13	3.46 ± 1.91	2.01 ± 1.62	1.21 ± 1.06
POA	8.15 ± 6.66	6.67 ± 7.71	6.39 ± 6.44	5.00 ± 5.19
SOA	10.58 ± 4.18	7.52 ± 3.80	6.11 ± 4.24	3.97 ± 3.26
O/C	0.61 ± 0.10	0.56 ± 0.12	0.53 ± 0.10	0.49 ± 0.11

human activities and other factors. The similar trend was also observed by the environmental monitoring sites of Ministry of Ecology and Environment (MEE) in Lanzhou. There are total five sites including four urban sites and one background site (Figure S1). The observed mass concentrations of air pollutants from these five sites are basically consistent. In this study, the results from Shengwusuo site that is closest to our sampling site is presented only (Figure 2c). The mass concentrations of $PM_{2.5}$ from this site during four periods were 63.7 ± 17.0 μg m^{-3}, 48.6 ± 18.0 μg m^{-3}, 36.4 ± 11.9 μg m^{-3}, and 33.8 ± 12.7 μg m^{-3}, respectively. The primary species of carbon monoxide (CO) also showed a decreased trend from P1 to P4 (1.6 ± 0.7 mg m^{-3} to 0.9 ± 0.5 g m^{-3}). Similar result was also observed for sulfur dioxide (SO_2), but the reduction was much smaller (P1 to P4: 18.8 ± 7.4 to 17.0 ± 8.9 μg m^{-3}). Note the mass concentrations of PM_{10} decreased from P1 to P2 (100.8 ± 26.5 to 72.3 ± 23.8 μg m^{-3}) but increased from P2 to P4 (102.4 ± 58.7 μg m^{-3}), likely due to influence of dust storm events. Satellite retrievals of NO_2 around Lanzhou during four periods showed similar results with that of ground records (Figure S9). The decreased mass concentration could also be illustrated by the size distribution of NR-PM_1 components, which were all shifted to smaller size (550 to 350 nm) from P1 to P4 (Figure 2e). This trend was also supported by SMPS measurement with lower number concentration and smaller size during P4 (Figure 2f). Due to the regular size cut of HR-ToF-AMS (D_{50} = 1,000 nm in vacuum aerodynamic diameter [D_{va}] and effectively $D_{50} \approx$ 750 nm in the physical diameter of the particle [D_p]) and smaller size cut for high aerosol density environment (Hu, Campuzano-Jost, et al., 2017), it seems that larger fraction of aerosol was missed by the AMS measurement during P1 (Figures 2e and S11), suggesting that the reduction in PM during control period might be even larger than measured.

The decreased PM concentration may closely be related with the reduction of primary emissions in these periods impacted by COVID-19 pandemic but also potentially influenced by meteorological conditions. In order to reduce the meteorological influences, a correction factor was calculated by comparing the concentration of CO at Shengwusuo site to that at the background site (Yuzhong, http://climate.lzu.edu.cn/) located ~30 km downwind of Lanzhou (Figure S1). The air quality of Yuzhong was heavily influenced by the outflow of Lanzhou (tight correlation of air pollutants between these two sites; Figure S10), and the station is built on a mountaintop (~500 m higher than Lanzhou) with little impacts from local emissions. The ratios of CO between these two stations could be treated as the diffusion rates during different periods. By normalizing to P1, the corrected factors were 1, 1.2, 1.2, and 1.12 for P1, P2, P3, and P4, respectively. The factor-corrected mass concentrations still decreased distinctly from P1 to P4. In addition, air temperature in Lanzhou between 2020 and the average values of 2013–2019 were comparable indicating similar variation of meteorological conditions and planetary boundary layer height (PBLH), while the concentrations of $PM_{2.5}$ and nitrogen dioxide (NO_2) were reduced significantly on 2020 after 2 weeks of the CNY compared with

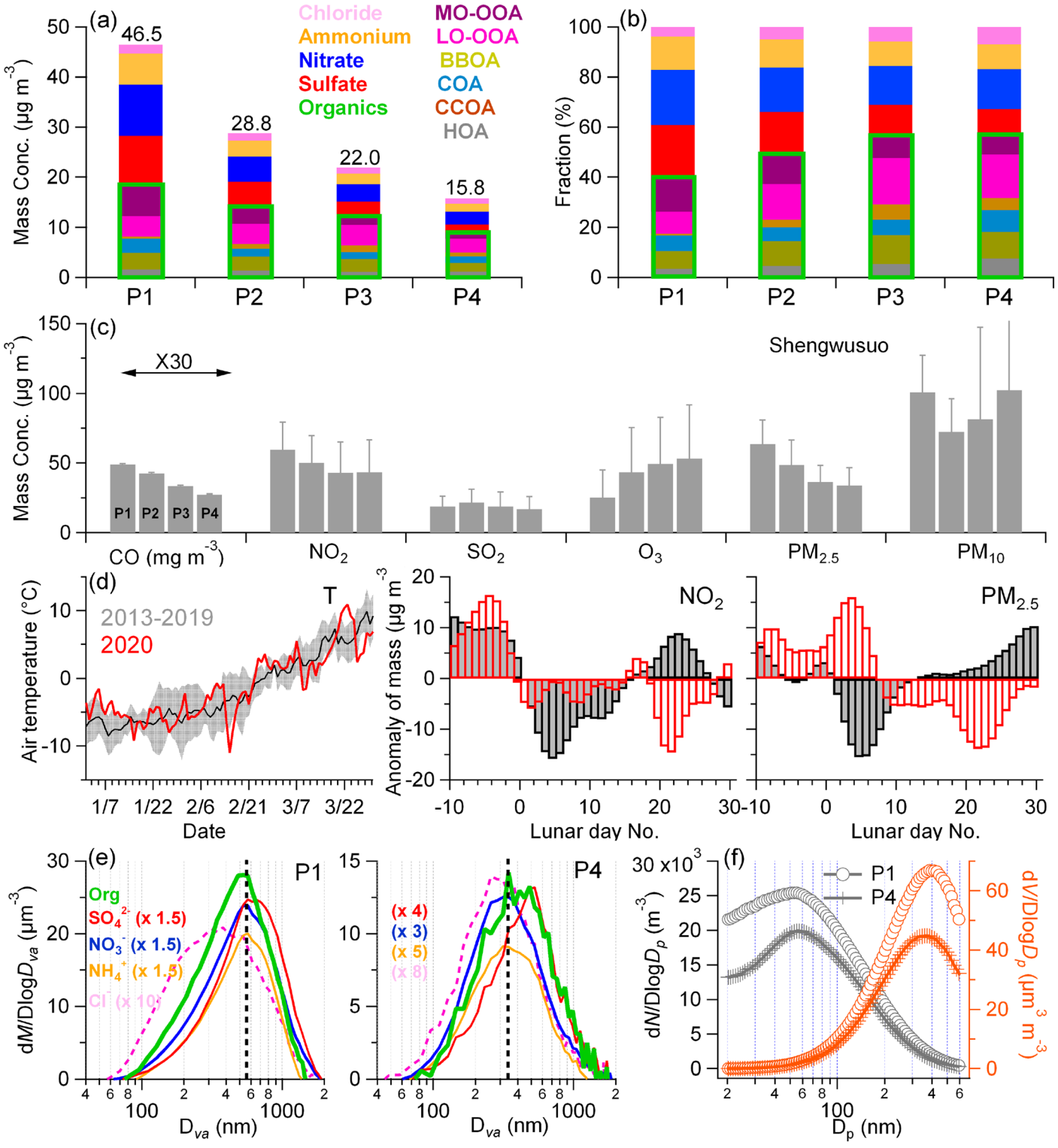

Figure 2. (a and b) Comparison between four periods for mass concentration and chemical composition, (c) chemical species from MME network site of Shengwusuo, (d) comparison of average profiles of the normalized daily variations of air temperature during 2013–2019 and 2020 relative to lunar day and NO_2 and $PM_{2.5}$ from January to March at Lanzhou, and (e and f) size distribution of AMS chemical components and SMPS number and volume concentration.

2013–2019 (Figure 2d). These results strongly suggest the reduction of PM concentration during P3 and P4 must be predominantly due to changes of emission and aerosol chemistry.

3.2. Variation of Chemical Composition and Sources During Different Periods

The chemical composition during four periods varied as well. During P1, NR-PM_1 consisted of 40.3% OA, and with important contributors of sulfate (20.5.7%), nitrate (22.1%), ammonium (13.3%), and chloride (3.8%), while the contributions of these species during P4 were 56.8% (OA), 10.5% (sulfate), 15.8% (nitrate), 10.0% (ammonium), and 6.9% (chloride), respectively. It is evident that the secondary inorganic species in total (sulfate, nitrate, chloride, and ammonium) were decreased significantly from P1 to P4 with a reduction rate of 47.5–75.5%, accounting for 68.4–74.6% of the total reduction of NR-PM_1. Note that the concentration of chloride was less reduced comparing with other inorganic species (less than 40%) and the mode of size distribution was at the smaller end of five components (Figure 2e), indicating that it was closely related with primary sources such as coal combustion (see below). The primary organic aerosol (POA, HOA + COA + BBOA + CCOA) also decreased from P1 to P4 with the total mass concentration of 8.1 μg m^{-3} at P1 to 5.0 μg m^{-3} at P4 with a somewhat smaller reduction rate of 18.3–38.7% during P2 and P4. However, variations of these POA components were different from each other. COA decreased significantly from 2.9 to 1.6 μg m^{-3} (P1 to P2) and further slightly decreased during P3 and P4 (to 1.4 μg m^{-3}). The HOA decreased from P1 to P2 (1.6 to 1.3 μg m^{-3}) but kept stable during P3 and P4 (1.2 μg m^{-3}). However, the total concentrations of BBOA and CCOA (indicating fuel usage) did not decrease; instead, they increased during P2 and P3 (~0.2 μg m^{-3}) than those during P1 but then decreased by 1.2 μg m^{-3} during P4 likely due to their reduced usage at a warmer condition. The secondary organic aerosol (SOA = LO-OOA + MO-OOA) concentration also declined from 10.6 (P1) to 4.0 μg m^{-3} (P4) with a reduction rate of 28.9–62.5% during P2 and P4. These results demonstrated that the reduction of NR-PM_1 concentration was dominated by secondary species.

4. Discussion

Based on the results above, it is evident that the concentration of PM during CNY and COVID-19 shutdown was reduced remarkably. The reduction rate of CO from P1 to P4 (44.1%) was comparable to the $PM_{2.5}$ (46.9%), but lower than that of NR-PM_1 (66.0%). The longer lifetime of CO and mineral dust components that were not accounted for in NR-PM_1 mass could partly offset the variations of CO and $PM_{2.5}$ (Cheng et al., 2016), whereas NR-PM_1 variation was dominated by reduction of secondary species. The drop of secondary species from P1 to P2–P4 could mainly be due to the reduction of primary precursors and/or low production rates. In this section below, we further investigated the behaviors of both secondary inorganic and organic species.

4.1. Secondary Inorganic Aerosol Species

The production rates of sulfate and nitrate during the four periods studied could be illustrated by the amplitude of their diurnal peaks. Figure 3a shows the diurnal variation of four species at four periods, which were subtracted by the minimum value and corrected with CO for each diurnal variation. The average diurnal patterns of all species were also shown in Figure S12. Sulfate and nitrate show a big drop for their peak from P1 to P4 (5–6 μg m^{-3}), whereas organics and chloride show a smaller gap between these periods (<1–4 μg m^{-3}). The production rates of sulfate and nitrate are further evaluated through two ratios, that is, $SOR = n_{sulfate}/\left(n_{SO_2} + n_{sulfate}\right)$ and $NOR = n_{nitrate}/(n_{NO_2} + n_{nitrate})$ (Figures 3b and 3c) (Xu et al., 2014). The data of SO_2 and NO_2 were taken from Shengwusuo site with 1 hr resolution. These two ratios were found to continuously decrease from P1 to P4 with decrease rates between P1 and P2–P4 of 61.3% for sulfate and 54.4% for nitrate, respectively. The potential impact of organosulfate (OS) and organonitrate (ON) on these calculations were also evaluated by calculating OS and ON based on methods in Chen et al. (2019) and Fry et al. (2013), respectively (Figure S13). The contribution of OS and ON to sulfate and nitrate were <10% in this study, and their impact on the calculation of SOR and NOR was therefore negligible. In contrast to the variations of SO_2 and NO_2 (Figure 3f), the decreases of sulfate and nitrate production rates were more significant, indicating that the overall capacity of SO_2 and NO_2 oxidations decreased. The ratios of SOR and NOR also showed a positive relationship with primary emission tracer CO, especially at low concentration range, which indicate the formation of sulfate and nitrate was highly sensitive to variations of primary emissions. The atmospheric

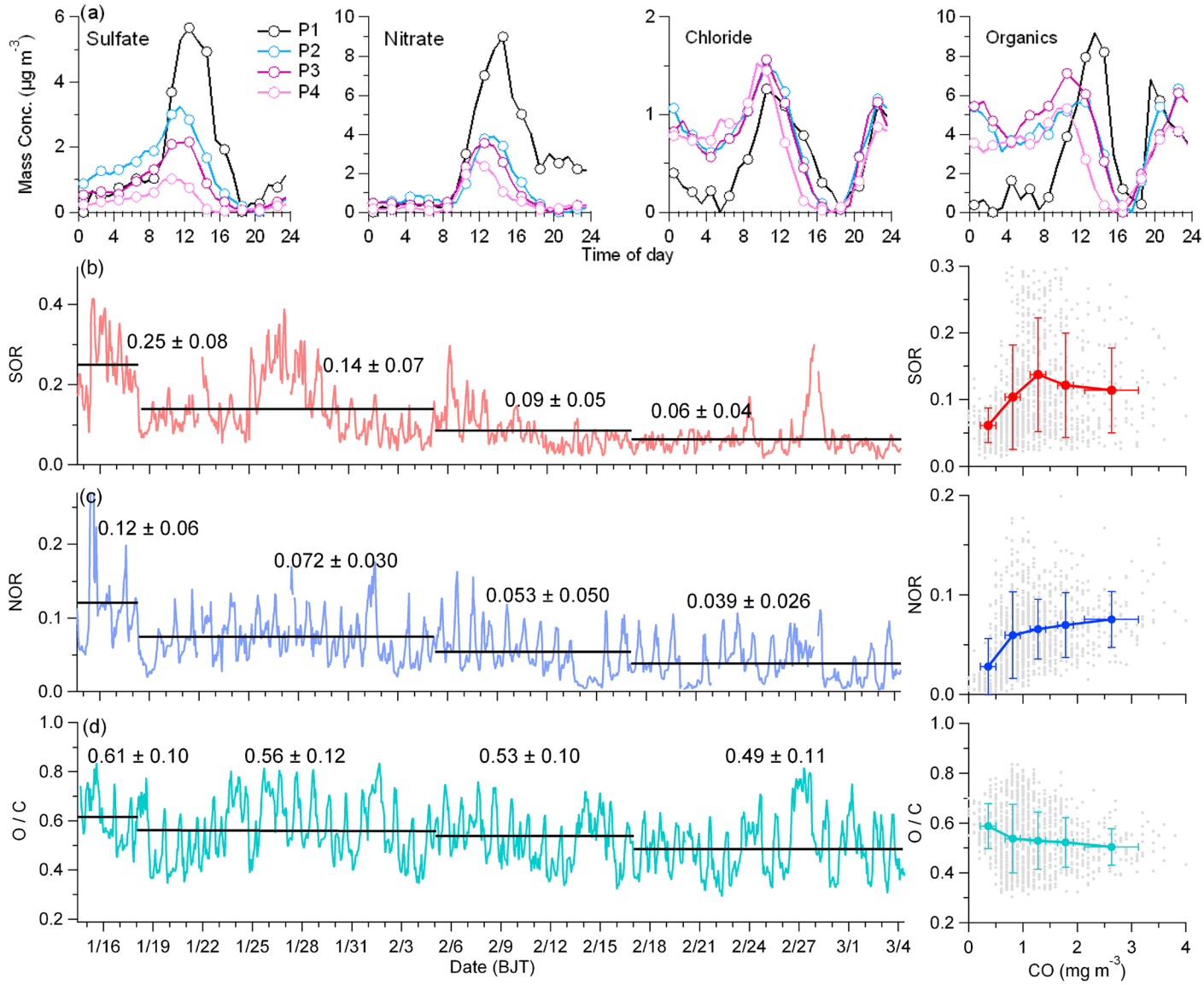

Figure 3. (a) The diurnal variations at four periods of different chemical species (sulfate, nitrate, chloride, and organics) and the production rate of (b) sulfate, (c) nitrate, and (d) oxygen-to-carbon (O/C) ratio of organics during four periods and relationship with primary species of carbon monoxide (CO). The diurnal variation at each period is subtracted by the minimum value and corrected by CO at each time point. The productions rate of SOR and NOR are defined as $SOR = n_{sulfate}/(n_{SO_2} + n_{sulfate})$ and $NOR = n_{nitrate}/(n_{NO_2} + n_{nitrate})$. SO_2 and NO_2 are from Shengwusuo site in Lanzhou.

oxidants (such as hydroxyl radicals) in atmosphere are in large part depending upon photochemical processes involved with nitrogen oxides (NOx = NO + NO_2) and volatile organic compounds (VOCs) (Stein and Saylor, 2012); therefore, in Lanzhou, reduction of these emissions may reduce its concentration, therefore the oxidation capacity. Indeed, the oxygen to carbon (O/C), an index of oxidation degree of OA, showed similar trend with those of SOR and NOR (Figure 3d).

It should be noted that our findings are in contrast with those observed in Eastern China. Huang et al. (2020) and Le et al. (2020) report that the mass concentrations of $PM_{2.5}$ in Beijing-Tianjin-Hebei area even slightly increased during early period of COVID-19 lockdown, and attributed it to that the production of secondary species offsets the reduction of primary emissions. High production efficiency of nitrate was also observed in Shanghai (Chang et al., 2020). The contrast between Lanzhou and Eastern China on aerosol formation could be due to adverse meteorological conditions in eastern China, such as low PBLH and calm wind (Le et al., 2020; Wang et al., 2020), but also aerosol precursors. For example, both anthropogenic and

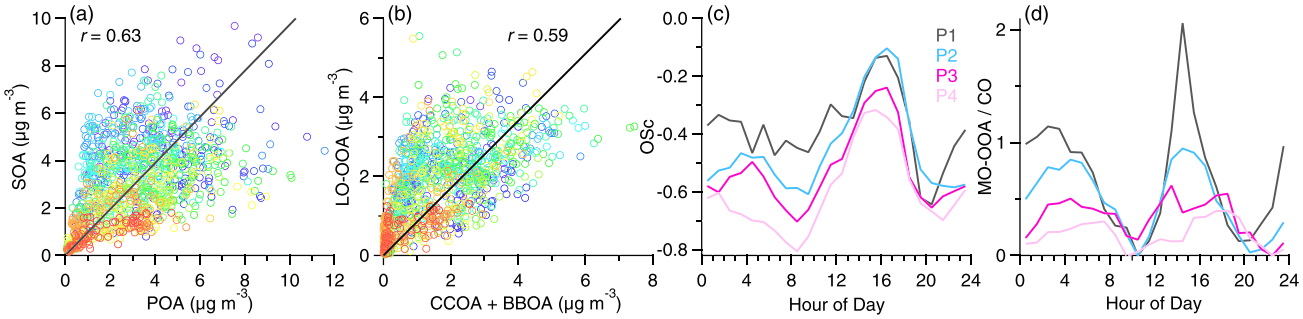

Figure 4. Scatter plots of (a) SOA versus POA, (b) LO-OOA versus CCOA + BBOA, (c) diurnal variation of carbon oxidation station (OSc) and during four periods, and (d) diurnal variation of MO-OOA subtracted by the minimum value and corrected by CO at each time point. In (a) and (b), the linear fittings of the data and Pearson's correlation coefficients (r) were shown.

biogenic emissions in eastern China are important sources and can promote the production of secondary aerosol, in contrast, anthropogenic emission (fossil fuel) is the dominated source in western China, such as in Lanzhou (Hu, Wang, et al., 2017).

4.2. Secondary Organic Aerosol Species

Similar to secondary inorganic aerosol species, the secondary organic aerosol species (SOA) variability may also relate to reduced emissions of its primary precursors and/or low production rates. We first checked on the relationship between POA and SOA and found a significant positive correlation between them ($r = 0.63$; Figure 4a), suggesting that the SOA reduction was closely associated with that of POA. In this study, the most significant reduction of POA was from COA and HOA (mainly COA). This result suggests that cooking emission may be an important source of SOA in Lanzhou. Previously, Xu et al. (2016) suggested that nonfossil fuel combustion emission including cooking and biomass burning emissions was an important original source of SOA based on radiation carbon isotope analysis. In details, cooking emissions can produce important precursors including alkenes, semivolatile and intermediate-volatility organic compounds, and they are important sources of SOA in urban areas (Liu et al., 2018).

Checking on the cross correlation between OA factors, it was found that LO-OOA was significantly correlated with CCOA + BBOA (Figure 4b). MO-OOA was weakly correlated with primary factors (Figure S14). Indeed, the temporal variation of LO-OOA was relatively stable compared to other OA components (Figure 1e). The decreased MO-OOA and stable LO-OOA suggest that a smaller fraction of LO-OOA was further oxidized to MO-OOA. Further, we checked on the oxidation state of OA using the carbon oxidation state (OSc) (Kroll et al., 2011), a useful metric for the degree of oxidation of organic species in the atmosphere (Figure 4c). The OSc varied between −1 and 0 for all the data and showed a decreased trend in their diurnal peaks from P1 to P4 (Figure 4c). This is consistent with the increased contribution of LO-OOA in SOA from P1 to P4 (Figure 1e). The diurnal variation of MO-OOA corrected by CO during four periods was also shown lower diurnal peaks from P2 to P4 compared with that of P1 (Figure 4d). These results may further indicate the lower atmospheric oxidation capacity after the COVID-19 lockdown. A bigger gap of OSc during four periods was observed at nighttime (0–8 a.m.), suggesting the dominating primary OA during P3 and P4 likely due to weak nocturnal heterogenic chemistry. The oxidants during nighttime such as nitrate radical (NO_3) is likely reduced due to the large reduction in NOx emission. Another potential reason for low concentration of radicals during P3 and P4 was likely from enhanced mineral dust mass loading during these periods, which could uptake these radicals, but not for ozone due to its low uptake efficiency (Tang et al., 2017). Overall, the SOA behavior in Lanzhou during the CNY and COVID-19 also showed a lower atmospheric oxidation capacity and was remarkably distinct from that in Eastern China (Huang et al., 2020).

5. Conclusions

Mass concentrations and chemical compositions of NR-PM_1 during January to March 2020 were obtained in Lanzhou using a HR-ToF-AMS and used to analyze the variations of aerosol mass concentrations and

potential sources during the different stages of the COVID-19 impacted period. The results show that the mass concentration of NR-PM_1 dropped by 50% from before to during control periods. This result was also supported by the data from MEE monitor stations in Lanzhou. The meteorological conditions, however, showed no significant variation in Lanzhou compared with the average of 2013–2019. Secondary inorganic components dominated the reduced mass concentration (70%), whereas the contribution of OA from coal combustion and biomass burning mainly for industry and residential heating was not reduced. The reduction of cooking and traffic emissions was on the other hand distinct during control period. In the meantime, the aerosol components were all shifted to smaller size during control period. We also found that the production rates of both secondary inorganic and organic aerosol components decreased during the control and recovery period, indicating a decrease of atmospheric oxidation capacity.

Overall, our findings here are in contrast with those observed in Eastern China, where oxidation capacity and production of secondary species were both enhanced and offset the reduction in primary emissions during COVID-19 lockdown. The strikingly different findings in Lanzhou clearly manifest that the governing aerosol chemical processes in Northwest China are distinct from those in Eastern China, which could be due to the regional difference on aerosol precursors between them (both anthropogenic and biogenic emissions in eastern China vs. anthropogenic emission in western China). This contrast could shed some lights on understanding of the mechanisms of aerosol production and further issue measures on air pollution control in these regions. Currently, it points out that strict control of primary emissions would be more effective in $PM_{2.5}$ alleviation in Lanzhou and other Northwestern cities than those in Eastern China, which provide important implications for the control measures of air pollution in this and similar northwest Chinese cities.

Data Availability Statement

The meteorological data in this study were from Urban Atmospheric Environmental Monitoring Data from the Key Laboratory of Land Surface Processes and Climate in Cold and Arid Regions, CAS. All the data in this manuscript are available at Zenodo (https://zenodo.org/record/3855067#.Xs8BFDl5vmE).

Acknowledgments

We would like to thank two anonymous reviewers for their constructive feeback and interest in our work. This research was supported by grants from the National Natural Science Foundation of China (41977189, 41771079, 41805106, and 41721091), the Key Laboratory of Cryospheric Sciences Scientific Research Foundation (SKLCS-ZZ-2020), and the Gansu Province Science and Technology Program (18JR3RA416).

References

Canagaratna, M. R., Jayne, J. T., Jimenez, J. L., Allan, J. D., Alfarra, M. R., Zhang, Q., et al. (2007). Chemical and microphysical characterization of ambient aerosols with the aerodyne aerosol mass spectrometer. *Mass Spectrometry Reviews*, *26*(2), 185–222. https://doi.org/10.1002/mas.20115

Canagaratna, M. R., Jimenez, J. L., Kroll, J. H., Chen, Q., Kessler, S. H., Massoli, P., et al. (2015). Elemental ratio measurements of organic compounds using aerosol mass spectrometry: Characterization, improved calibration, and implications. *Atmospheric Chemistry and Physics*, *15*(1), 253–272. https://doi.org/10.5194/acp-15-253-2015

Canonaco, F., Crippa, M., Slowik, J. G., Baltensperger, U., & Prévôt, A. S. H. (2013). SoFi, an IGOR-based interface for the efficient use of the generalized multilinear engine (ME-2) for the source apportionment: ME-2 application to aerosol mass spectrometer data. *Atmospheric Measurement Techniques*, *6*(12), 3649–3661. https://doi.org/10.5194/amt-6-3649-2013

Chang, Y., Huang, R. J., Ge, X., Huang, X., Hu, J., Duan, Y., et al. (2020). Puzzling haze events in China during the coronavirus (COVID-19) shutdown. *Geophysical Research Letters*, *47*, e2020GL088533. https://doi.org/10.1029/2020GL088533

Chen, Y., Xu, L., Humphry, T., Hettiyadura, A. P. S., Ovadnevaite, J., Huang, S., et al. (2019). Response of the aerodyne aerosol mass spectrometer to inorganic sulfates and organosulfur compounds: Applications in field and laboratory measurements. *Environmental Science and Technology*, *53*(9), 5176–5186. https://doi.org/10.1021/acs.est.9b00884

Cheng, Y., Zheng, G., Wei, C., Mu, Q., Zheng, B., Wang, Z., et al. (2016). Reactive nitrogen chemistry in aerosol water as a source of sulfate during haze events in China. *Science Advances*, *2*(12), e1601530. https://doi.org/10.1126/sciadv.1601530

DeCarlo, P. F., Kimmel, J. R., Trimborn, A., Northway, M. J., Jayne, J. T., Aiken, A. C., et al. (2006). Field-deployable, high-resolution, time-of-flight aerosol mass spectrometer. *Analytical Chemistry*, *78*(24), 8281–8289. https://doi.org/10.1021/ac061249n

Fry, J. L., Draper, D. C., Zarzana, K. J., Campuzano-Jost, P., Day, D. A., Jimenez, J. L., et al. (2013). Observations of gas- and aerosol-phase organic nitrates at BEACHON-RoMBAS 2011. *Atmospheric Chemistry and Physics*, *13*(17), 8585–8605. https://doi.org/10.5194/acp-13-8585-2013

Hu, J., Wang, P., Ying, Q., Zhang, H., Chen, J., Ge, X., et al. (2017). Modeling biogenic and anthropogenic secondary organic aerosol in China. *Atmospheric Chemistry and Physics*, *17*(1), 77–92. https://doi.org/10.5194/acp-17-77-2017

Hu, W., Campuzano-Jost, P., Day, D. A., Croteau, P., Canagaratna, M. R., Jayne, J. T., et al. (2017). Evaluation of the new capture vaporizer for aerosol mass spectrometers (AMS) through field studies of inorganic species. *Aerosol Science and Technology*, *51*(6), 735–754. https://doi.org/10.1080/02786826.2017.1296104

Huang, X., Ding, A., Gao, J., Zheng, B., Zhou, D., Qi, X., et al. (2020). Enhanced secondary pollution offset reduction of primary emissions during COVID-19 lockdown in China. *National Science Review*, nwaa137. https://doi.org/10.1093/nsr/nwaa137

Jayne, J. T., Leard, D. C., Zhang, X., Davidovits, P., Smith, K. A., Kolb, C. E., & Worsnop, D. R. (2000). Development of an aerosol mass spectrometer for size and composition analysis of submicron particles. *Aerosol Science and Technology*, *33*(1–2), 49–70. https://doi.org/10.1080/027868200410840

Kroll, J. H., Donahue, N. M., Jimenez, J. L., Kessler, S. H., Canagaratna, M. R., Wilson, K. R., et al. (2011). Carbon oxidation state as a metric for describing the chemistry of atmospheric organic aerosol. *Nature Chemistry*, *3*(2), 133–139. https://doi.org/10.1038/nchem.948

Kuwata, M., Zorn, S. R., & Martin, S. T. (2011). Using elemental ratios to predict the density of organic material composed of carbon, hydrogen, and oxygen. *Environmental Science and Technology*, *46*(2), 787–794. https://doi.org/10.1021/es202525q

Le, T., Wang, Y., Liu, L., Yang, J., Yung, Y. L., Li, G., & Seinfeld, J. H. (2020). Unexpected air pollution with marked emission reductions during the COVID-19 outbreak in China. *Science*, *369*(6504), 702–706. https://doi.org/10.1126/science.abb7431

Liu, T., Wang, Z., Huang, D. D., Wang, X., & Chan, C. K. (2018). Significant production of secondary organic aerosol from emissions of heated cooking oils. *Environmental Science & Technology Letters*, *5*(1), 32–37. https://doi.org/10.1021/acs.estlett.7b00530

Paatero, P., & Tapper, U. (1994). Positive matrix factorization: A non-negative factor model with optimal utilization of error estimates of data values. *Environmetrics*, *5*(2), 111–126. https://doi.org/10.1002/env.3170050203

Stein, A. F., & Saylor, R. D. (2012). Sensitivities of sulfate aerosol formation and oxidation pathways on the chemical mechanism employed in simulations. *Atmospheric Chemistry and Physics*, *12*(18), 8567–8574. https://doi.org/10.5194/acp-12-8567-2012

Tang, M., Huang, X., Lu, K., Ge, M., Li, Y., Cheng, P., et al. (2017). Heterogeneous reactions of mineral dust aerosol: Implications for tropospheric oxidation capacity. *Atmospheric Chemistry and Physics*, *17*(19), 11,727–11,777. https://doi.org/10.5194/acp-17-11727-2017

Tian, H., Liu, Y., Li, Y., Wu, C.-H., Chen, B., Kraemer, M. U. G., et al. (2020). An investigation of transmission control measures during the first 50 days of the COVID-19 epidemic in China. *Science*, *368*(6491), 638–642. https://doi.org/10.1126/science.abb6105

Ulbrich, I. M., Canagaratna, M. R., Zhang, Q., Worsnop, D. R., & Jimenez, J. L. (2009). Interpretation of organic components from positive matrix factorization of aerosol mass spectrometric data. *Atmospheric Chemistry and Physics*, *9*(9), 2891–2918. https://doi.org/10.5194/acp-9-2891-2009

Wang, P., Chen, K., Zhu, S., Wang, P., & Zhang, H. (2020). Severe air pollution events not avoided by reduced anthropogenic activities during COVID-19 outbreak. *Resources, Conservation and Recycling*, *158*, 104814. https://doi.org/10.1016/j.resconrec.2020.104814

Xu, J., Shi, J., Zhang, Q., Ge, X., Canonaco, F., Prévôt, A. S. H., et al. (2016). Wintertime organic and inorganic aerosols in Lanzhou, China: Sources, processes, and comparison with the results during summer. *Atmospheric Chemistry and Physics*, *16*(23), 14,937–14,957. https://doi.org/10.5194/acp-16-14937-2016

Xu, J., Zhang, Q., Chen, M., Ge, X., Ren, J., & Qin, D. (2014). Chemical composition, sources, and processes of urban aerosols during summertime in Northwest China: Insights from high-resolution aerosol mass spectrometry. *Atmospheric Chemistry and Physics*, *14*(23), 12,593–12,611. https://doi.org/10.5194/acp-14-12593-2014

Zhang, Q., Canagaratna, M. R., Jayne, J. T., Worsnop, D. R., & Jimenez, J. L. (2005). Time- and size-resolved chemical composition of submicron particles in Pittsburgh: Implications for aerosol sources and processes. *Journal of Geophysical Research*, *110*, D07S09. https://doi.org/10.1029/2004JD004649